Aeromonas proteolytica Aminopeptidase: An Investigation of the Mode of Action Using a Quantum Mechanical/Molecular Mechanical Approach†

Gudrun Schürer, Harald Lanig, and Timothy Clark*

Computer-Chemie-Centrum, Friedrich-Alexander-Universität Erlangen-Nürnberg, Nägelsbachstrasse 25, 91052 Erlangen, Germany

Received January 7, 2003; Revised Manuscript Received March 10, 2004

ABSTRACT: The aminopeptidase of *Aeromonas proteolytica* (AAP) belongs to the group of metallohydrolases that require two divalent cations for full activity. Such binuclear metal centers are found in several aminopeptidases, raising the question whether a common mechanism, at least partly, is likely. We have used a quantum mechanical/molecular mechanical (QM/MM) approach to investigate the reaction mechanism of AAP. Among several possibilities, one reaction path was found to be clearly the most favorable. Beside the chemical transformation steps, effects of the enzyme environment and the influence of the solvent on the catalytic reaction were included in the study. The results are in good agreement with experimental studies and correspond to a high degree to our previous QM/MM calculations on the reaction mechanism of the related binuclear bovine lens leucine aminopeptidase (blLAP), which, although related to the AAP, has different Zn^{2+}-coordination spheres and a different catalytic residue. The mechanisms of the two enzymes as suggested in the literature differ on the mode of coordination of the nucleophile and the identity of the general base. However, the results of this and our previous work on blLAP allow us to identify a common mechanism for the two enzymes. This mechanism is probably quite general for binuclear zinc enzymes.

Computational studies on enzyme reaction mechanisms may serve two purposes, either to reproduce the kinetics of the enzymatic reaction as closely as possible and to identify the exact source of the enzymatic catalysis or, as in the case of the present study, to identify the most likely reaction mechanism and to try to find common mechanistic principles for classes of enzymes. This work is designed to provide a general mechanistic framework for the binuclear zinc hydrolases by studying two examples of these enzymes. In a previous paper, we examined the reaction mechanism of the bovine lens leucine aminopeptidase (*1*), and we have now examined the aminopeptidase from *Aeromonas proteolytica*.

Aminopeptidases catalyze the cleavage of the N-terminal amino acid residue of proteins and peptides. They are widely distributed in bacteria, yeast, plant, and animal tissues and are of critical biological and medical importance. Their functions include protein maturation and degradation, hormone level regulation, and cell-cycle control. Abnormal aminopeptidase activity has been associated with pathological disorders such as cataracts, inflammation, cancer, and leukemia (*2*). The inhibition of leucine aminopeptidase by bestatin, a naturally occurring peptide analogue inhibitor, was shown to decrease human immunodeficiency virus (HIV) viral load (*3*). An understanding of the catalytic mechanism of these important enzymes would help to develop effective inhibitors.

Bacterial aminopeptidases are of interest to the agro and dairy industries. Almost half of these enzymes are monomers, while the remainder have oligomeric structures. For the most part, they show Michaelis−Menten kinetics (*4*). The largest group, about two-thirds, are metallo-aminopeptidases that need at least one divalent cation, most frequently Zn^{2+} (*5*), as a cofactor. Some, such as the *Escherichia coli* methionine aminopeptidase (*6*), containing two Co^{2+} ions, and the *E. coli* aminopeptidase A (PepA, *7*), containing two Zn^{2+} ions, have binuclear metal centers (*8*). The active site of PepA is isostructural to the active site of leucine aminopeptidase from bovine lens (blLAP,[1] *9*). The aminopeptidases of *Aeromonas proteolytica* (AAP) and *Streptomyces griseus* (SGAP) are also related to blLAP. These enzymes display high thermostability, and their activity is strongly inhibited by bestatin.

The Protein Data Bank (*10*) includes several 3D structures of AAP: the native enzyme (1AMP, *11*), the complex with the metal chelator *p*-iodo-D-phenylalanine hydroxamate (1IGB, *12*), the complex with 1-butaneboronic acid (1CP6, *13*), and the complex with the transition-state analogue L-leucine phosphonic acid (1FT7, *14*). AAP is a small, monomeric enzyme (32 kDa) with a substrate specificity for hydrophobic residues. It folds into a single α/β globular domain. A central twisted β-sheet sandwiched between α-helices forms the hydrophobic core of the protein. Despite a low level of amino acid identity, AAP and the catalytic domain of blLAP have homologous folds. The well-defined catalytic pocket is located at the surface of the protein and

† This study was supported by the Deutsche Forschungsgemeinschaft.

* To whom correspondence should be addressed. E-mail: clark@chemie.uni-erlangen.de.

[1] Abbreviations: AAP, *Aeromonas proteolytica* leucine aminopeptidase; blLAP, bovine lens leucine aminopeptidase; BuBA, 1-butaneboronic acid; DFT, density-functional theory; IPH, *p*-iodo-D-phenylalanine hydroxamate; LPA, L-leucine phosphonic acid; QM/MM, quantum mechanical/molecular mechanical; SGAP, *Streptomyces griseus* leucine aminopeptidase.

10.1021/bi0340191 CCC: $27.50
Published on Web 04/16/2004

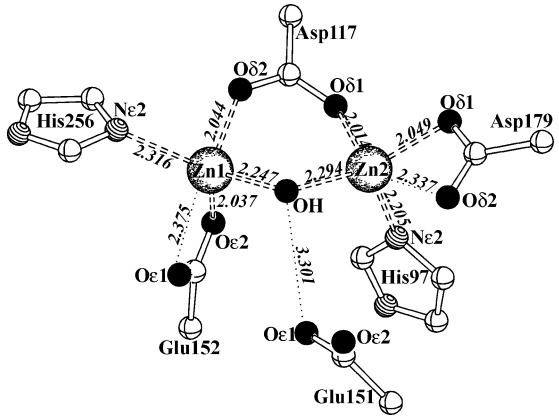

FIGURE 1: Active site of the AAP taken from PDB entry 1AMP. The distances are given in Å.

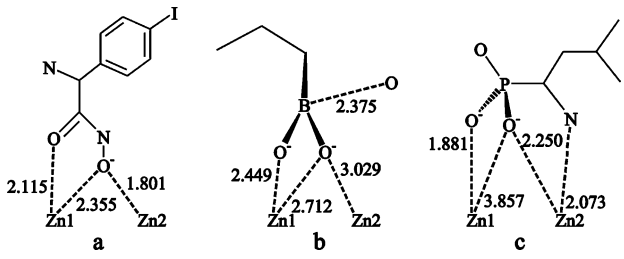

FIGURE 2: Inhibitor binding modes of AAP with (a) *p*-iodo-D-phenylalanine hydroxamate (IPH), (b) 1-butaneboronic acid (BuBA), and (c) L-leucine phosphonic acid (LPA). The distances are given in Å and are taken from the X-ray structures.

its hydrophobic character reflects the preference of AAP for hydrophobic amino-terminal residues. An uncommon feature is the appearance of a cis peptide bond between Asp117, which is a part of the active site, and Asp118 (*11*).

The active site (see Figure 1) is located in a loop region near the edge of the binding pocket. It consists of two Zn^{2+} ions, each coordinated with a histidine and an aspartate or a glutamate. Additionally, an aspartate and a water molecule or hydroxide ion bridge the two metal ions. These have equivalent structural environments, suggesting a symmetrical role in catalysis. Both Zn^{2+} ions have approximately tetrahedral coordination polyhedra if the weak interaction to the second oxygen atoms of the carboxylate ligands is neglected (*11*). The coordination stereochemistry for all Zn^{2+}−ligand interactions (syn and in-plane for carboxylate and head-on for histidine) is in agreement with observed zinc binding preferences (*15*). An additional glutamate residue (Glu151) is located near the active site, in structural analogy to the metallo-peptidases thermolysin and carboxypeptidase A. It has been suggested to play the role of a general base in the catalytic reaction. This residue is hydrogen bonded to the bridging water/hydroxide (*12*).

The inhibitor-binding mode (see Figure 2a) in the complex with *p*-iodo-D-phenylalanine hydroxamate (IPH, PDB entry 1IGB) shows similarities to that of mononuclear metallo-peptidase−hydroxamate complexes, because the hydroxamate is a bidentate ligand to Zn1 via its carbonyl and hydroxy oxygens. At the same time, the deprotonated hydroxy group replaces the bridging water/hydroxide and in this way is coordinated to Zn2. Additionally, the hydroxamate hydroxy oxygen interacts with Glu151, which must be protonated to allow a hydrogen bridge. A hydrogen bond between the amino group of the inhibitor and Tyr225 contributes further to the stabilization of the complex (*12*). Because of the wrong stereochemistry (the inhibitor has the D-configuration and AAP cleaves N-terminal L-amino acids), it is questionable whether the binding mode of IPH allows conclusions about the binding mode of natural substrates (*14*).

The complex with the competitive inhibitor 1-butaneboronic acid (BuBA) (PDB entry 1CP6, see Figure 2b) can be regarded as a snapshot of the proteolytic reaction at a stage between the Michaelis complex and the transition state. BuBA only binds to Zn1. Interestingly, the boron atom clearly is not sp^2- but sp^3-hybridized. A water molecule that is not present in the native structure was found at a distance of 2.4 Å from the boron, but no water is coordinated to the Zn^{2+} ions. The new water is suggested to be the former bridging ligand that first lost its Zn2 coordination and was then released from Zn1 as a result of the inhibitor binding. Presumably, it also changes the hybridization of the boron atom from sp^2 to sp^3 by interacting with the unoccupied boron p-orbital (*13*).

The complex with L-leucine phosphonic acid (LPA) (PDB entry 1FT7) is a transition state analogue complex (see Figure 2c). The phosphonate group is coordinated via one oxygen to each of the Zn^{2+} ions. The Zn2-bound oxygen has a hydrogen bond to Glu151. There is no single ligand atom bridging the two metal ions. Additionally, the N-terminal amino group is coordinated to Zn2. LPA binding, like the binding of IPH and BuBA, does not induce significant conformational changes in the protein (*14*).

Kinetic (*14*, *16*) and spectroscopic (*14*, *17*−*20*) studies have been performed on AAP. A catalytic mechanism was proposed on the basis of these and the crystallographic data (see Figure 3). The substrate peptide binds to Zn2 with its N-terminal amino group and to Zn1 with the carbonyl oxygen of the scissile peptide bond. Additionally, the N-terminus interacts with Asp179. Upon substrate binding, the bridging water molecule loses its coordination to Zn2 and becomes terminally bound to Zn1. The coordination cleavage is assisted by a hydrogen bond from Asp99 to Nδ1 of the Zn2-ligand His97. Such carboxylate−histidine−metal triads can be found in several zinc-containing enzymes (*21*). Furthermore, Glu151 is also suggested to contribute to the regulation of the Lewis acidity of Zn2 by a hydrogen bond to the Zn2-coordinated His97-Nϵ2 (*14*). However, the active site topology suggests that Glu151-Hϵ1 of the protonated glutamate must be perpendicular to the carboxyl plane to be reasonably positioned for a hydrogen bond. This would be a very unlikely conformation. A hydrogen bond between the terminal water molecule and Glu151 allows deprotonation of the former to give a hydroxide ion as nucleophile. The nucleophilic attack results in the tetrahedral intermediate, which is coordinated to Zn1. The neutral Glu151 may act as a proton donor for the peptide nitrogen. The rate-limiting step is probably the C−N-breaking step, that is, the product formation (*14*, *16*). Studies on thiol- or aliphatic alcohol-containing inhibitors (*22*−*24*) and on the hydrolysis of thionopeptides (*25*) indicate that the initial step of the substrate binding is the interaction of the N-terminal amino acid moiety with the hydrophobic pocket followed by carbonyl binding to Zn1. Subsequently, the N-terminal amino group interacts with Zn2.

The catalytic mechanism suggested for the AAP by Stamper et al. (*14*) corresponds for the most part to the

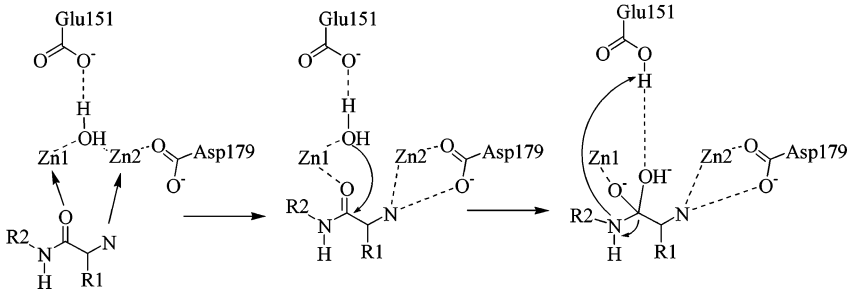

FIGURE 3: Scheme of the catalytic mechanism suggested by Stamper et al.

results of our previous study on the reaction mechanism of the related blLAP (*1*), which also requires two Zn^{2+} ions for full activity (*26*). However, the coordination sphere of the blLAP is different from that of the AAP. Most of the ligands are carboxylates, one is a lysine, and one is a backbone carbonyl oxygen. Moreover, unlike the AAP, the Zn^{2+} ions in the blLAP occupy different environments, and there is a catalytic lysine (Lys262) in the active site (*27*). In the suggested reaction mechanism, which is based on structures of transition state analogue complexes, the nucleophilic water attacks the carbonyl carbon of the substrate from a position bridging the two metal ions (*28*). Because the X-ray structure of the homologous PepA shows a carbonate ion near the active site, this ion was suggested to play the role of the general base that deprotonates the water molecule and protonates the peptide nitrogen (*9*). Lys262, which we found to correspond to Glu151 in the AAP, was not favored as the proton donor for the peptide nitrogen. Note that, despite the fact that the decomposition of the tetrahedral intermediate is proposed to be rate-limiting, this intermediate has not been observed experimentally because no enzyme−substrate complexes are stable.

The aim of this study is to gain insight into the catalytic mechanism of the AAP on a molecular level. Comparison with the related binuclear zinc-hydrolase blLAP allows us to propose a common mode of action for this class of enzymes. A further aim is to investigate the entire reaction, including the coordination of the substrate to and the decoordination of the products from the metal ions, rather than only the chemical transformation. As for the catalytic reaction, the system offers various possibilities for the formation and cleavage of the Zn^{2+} coordination, which can be regarded as the initial and final steps of the chemical reaction.

METHODS

QM/MM techniques, first introduced and developed by Warshel and co-workers in 1976 (*29*), have been widely used to investigate enzyme reaction mechanisms (*30*). They allow a quantum mechanical description of the active site, which is essential for investigating chemical reactions, and a simultaneous consideration of important long-range effects of the enzyme environment. A reasonable active site model of the AAP, even without any substrate, includes six residues (120 atoms). High-level ab initio or DFT calculations give accurate results, but the computational costs required for a comprehensive investigation of a model system of this size are far too high. Therefore, we chose a semiempirical/molecular mechanical approach. Although semiempirical MO techniques are not generally regarded as state-of-the-art for the investigation of chemical reaction mechanisms, they are nonetheless still the best way to treat a model system large enough to allow the study of important geometrical changes within the coordination sphere of the metal-containing active site of an enzyme. Their speed allows far more comprehensive investigations of alternative reaction paths and the use of a large quantum mechanical system that moves the QM/MM boundary away from the active site. Nevertheless, the possible inaccuracies of the semiempirical methods should be kept in mind. In a study of the hydrolysis mechanism of formamide with various theoretical methods, Antonczak et al. showed that AM1 overestimates the activation energies but gives qualitatively similar results to higher level methods (*31*). Investigations intended to give a quantitative picture of a chemical reaction require the free energy to be calculated. One such approach based on calibrated and validated parameters for the corresponding reaction in water (*32*) is Warshel's empirical valence bond (EVB) method (*33*). However, our study is not intended to predict exact energies but rather to investigate the probability of different reaction paths by comparing the semiempirical energies. In this way, systematic errors cancel to a high degree, although the accuracy of the calculated activation barriers certainly is not adequate.

Computational Details. A detailed description of the QM/MM method is given in our earlier paper on the reaction mechanism of the blLAP (*1*). The QM and MM part interactions include the Coulomb and van der Waals contributions. The QM polarization by the MM environment is taken into account by the perturbation of the one-center Fock matrix. There are no covalent bonds across the QM/MM boundary. If not denoted otherwise, the energies given are the total energies, which include the QM and MM energies of the two subsystems, the Coulomb interaction energy, and the van der Waals interaction energy.

All calculations were performed with the semiempirical program package VAMP 7.5 (*34*). The Tripos force field (*35*) implemented in VAMP was used for the treatment of the MM part. Parameters that were missing in the original implementation were set using the published algorithm (*36*). Missing atom parameters were taken from the Sybyl program. No cutoff values were used for the calculation of van der Waals and Coulomb energies because this can cause energy discontinuities during geometry optimizations. The QM part was treated with the AM1 Hamiltonian (*37*) and the zinc parameters of Dewar and Merz (*38*). The zinc parameters were tested for their suitability for multinuclear centers in our earlier study (*1*). For the QM/MM calculations, we chose an alternating optimization strategy, allowing the MM part to relax to the changes in the QM part to avoid

too many time-consuming QM calculations. All structures were optimized to consistency of both subsystems (0.4 kcal mol^{-1} $Å^{-1}$ for the QM part). For the MM optimization, we used a low-memory Broyden−Fletcher−Goldfarb−Shanno (BFGS) algorithm (*39*), and for the QM optimization, we used the eigenvector following method (*40*). The local minima and transition states were characterized by calculating the normal modes. Further details of the parameters used to perform the calculations are available from the authors.

For the stationary points along the most favorable reaction path obtained with the QM/MM method, higher level energies were calculated using DMol[3] (*41*) implemented in the program package Materials Studio (*42*). We used the Perdew−Wang 91 functional and a double numerical plus polarization basis set (PW91/DNP) (*41*, *43*). This combination of functional and basis set should give reliable results and is computationally more economical than hybrid density-functional techniques (*44*).

System Preparation. Sybyl 6.6 (*36*) was used for the preparation of the input files. Both the QM and the MM parts must be intact systems, so the total system must be divided and the fragments saturated with hydrogen link atoms. The QM part contains the substrate model, the metal ions, and the active site residues; the MM part contains the enzyme bulk and the crystal water molecules of the PDB entry. The two subsystems were separated by cutting the backbone within the residues next to the amino acids included in the QM system. The cut was made between the C_α-atom and the peptide nitrogen at the N-terminus or the carbonyl carbon at the C-terminus of the fragment, leaving the peptide bonds in the QM part. The C_α- and H_α-atoms in the MM part were deleted, and the resulting amino acid fragments and the remaining side chains that are no longer connected to the protein backbone were saturated with hydrogens (a schematic representation of the separation procedure is given in the Supporting Information as Figure S1). The electrostatic and van der Waals interactions to the surrounding protein, together with weak harmonic constraints (with force constants of 10−20 kcal mol^{-1} $Å^{-2}$) on the peptide C- and N-atoms of the backbone to their X-ray positions, ensure that the resulting QM model system retains its position within the MM part. Additionally, to avoid artificial repulsive interactions between MM and QM parts causing large forces, the radii of the link hydrogens were reduced to 0.1 Å. The separation procedure has been validated and used successfully in studies on phospholipase A_2 (*45*) and blLAP (*1*). The point charges of the MM environment were generated by the Gasteiger−Marsili method (*46*). The total charge of the MM part should ideally be zero to avoid large forces on charged active site residues. Therefore, as many glutamate or aspartate residues as necessary positioned at the protein surface as far away from the binding pocket as possible were protonated to neutralize the charge. To ensure that there were no large initial gradients, the environment was relaxed with the tetrahedral intermediate in the QM part. The relaxed environment was then used as a starting geometry for further calculations.

The QM/MM Model Systems. The inputs were based on the X-ray structure 1FT7. The tetrahedral intermediate of a Leu-Ala dipeptide as a substrate model can be generated easily from the transition state analogue L-leucine phosphonate. To avoid interactions of active site residues with the C-terminal carboxyl or carboxylate group, which is not present in a natural substrate, the C-terminus was blocked with a methyl group after the alanine carbonyl carbon. The 3D-structures of the model systems are available from the authors.

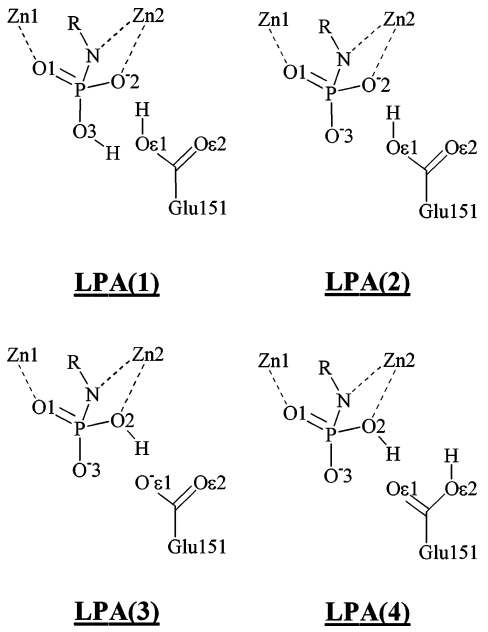

FIGURE 4: Schematic representation of the active site of the LPA−AAP complex in different protonation states (**LPA(1−4)**).

The QM system for most calculations on AAP includes the two Zn^{2+} ions, the inhibitor LPA or the methyl-blocked Leu-Ala dipeptide, His97, Asp117, Glu151, Glu152, Asp179, and His256. For some studies, a system extended by Asp99, Cys227, and Ser228 or by Tyr225 was also used, which is then denoted in the text.

RESULTS

Optimization of the LPA−AAP Complex

The X-ray structure 1FT7 does not show the protonation state of the phosphonate group of the inhibitor LPA. Because the second pK_a value of phosphonic acid is 6.7 (*47*), the L-leucine phosphonate probably has a charge of −2 at pH 8. However, this pK_a value depends on the environment and substituents to a high degree. Therefore, to investigate the protonation state of LPA and to validate our calculational approach especially with respect to the Zn^{2+}−ligand coordination distances, the LPA−AAP complex was optimized as described above. Because Tyr225 is involved in inhibitor binding in the IPH−AAP complex (PDB entry 1IGB), this residue was included in the QM system. However, no interaction of Tyr225 to LPA or any other active site residue was found in either of the calculated systems.

The short distance (2.380 Å) between the Zn2-coordinated phosphonate oxygen and Glu151-Oϵ1 in the X-ray structure indicates a hydrogen bridge, so either the phosphonate or the carboxylate oxygen must be protonated. Four systems with reasonable protonation states were optimized (see Figure 4). **LPA(1)** can only be compared directly with **LPA(4)** and **LPA(2)** with **LPA(3)** because these pairs are exactly isomeric. Although we calculate the systems with the unprotonated phosphonate oxygen O2 to be 20.3 kcal mol^{-1}

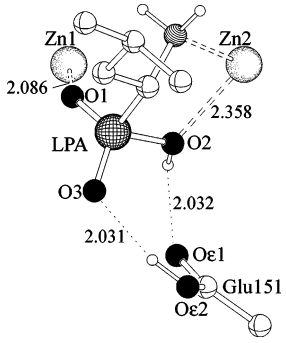

FIGURE 5: Active site of the optimized LPA−AAP complex **LPA-(4)**. Distances are given in Å.

(LPA(1)) and 26.8 kcal mol^{-1} **(LPA(2))** lower in energy than the corresponding structures, the RMS deviations of the systems **LPA(4)** and **LPA(3)** with a protonated O2 are considerably smaller. Furthermore, the X-ray structure shows a difference of 0.369 Å in the coordination distances Zn1−O1 and Zn2−O2, indicating strongly that O2 is protonated. The X-ray structure also shows that LPA-O2 interacts with Glu151-Oϵ1 and, although more weakly, with Glu151-Oϵ2, but there is no hydrogen bond between LPA-O3 and Glu-Oϵ2. **LPA(3)** reflects this pattern well, but in **LPA(4)**, the interaction between LPA-O2 and Glu151-Oϵ2 is missing. Instead, there is a hydrogen bond between LPA-O3 and Glu151-Oϵ2. However, the RMS deviation of **LPA(4)** is slightly smaller than that of **LPA(3)**, and taking Glu151 as a possible proton donor into account, **LPA(4)** represents the most likely protonation state. The optimized system **LPA(4)** (see Figure 5) shows two hydrogen bonds between the phosphonate group and the protonated Glu151.

AM1 tends to overestimate the Zn^{2+}−Zn^{2+} and the Zn^{2+}−ligand distances to oxygen atoms, whereas the Zn^{2+}−nitrogen distances are slightly smaller for the histidine ligands. These results are in good agreement with our earlier study on multinuclear Zn^{2+} complexes (*1*). The coordination distance to the N-terminal amino group is larger. However, the corresponding distance in the LPA−blLAP complex (PDB entry 1LCP) is 0.208 Å longer than that in the LPA−AAP complex, suggesting some error in the X-ray structure. Furthermore, the hydrogen bonding distances of the optimized structure are longer than the corresponding X-ray structure distances. This effect is known and has been investigated by Zheng and Merz (*48*).

The optimizations of the LPA−AAP complexes show that, within the scope of known systematic deviations, the QM/MM method and the AM1 Hamiltonian are suitable for describing the AAP active site. Furthermore, they indicate that **LPA(4)** with O2 and Glu151-Oϵ2 protonated probably represents the protonation pattern found in the X-ray structure of the LPA−AAP complex. A detailed list of relevant atomic distances of the optimized systems **LPA(1−4)** is given in the Supporting Information (Table S1).

Optimization of the Leu-Ala−AAP Complex

Although some assumptions concerning the reaction mechanism of the peptide hydrolysis (e.g., that it is a general base mechanism that proceeds via a tetrahedral intermediate) can be considered as true, there are a number of reaction possibilities to be investigated. The notation used for structures occurring during the alternative reaction paths is given in Figure 6.

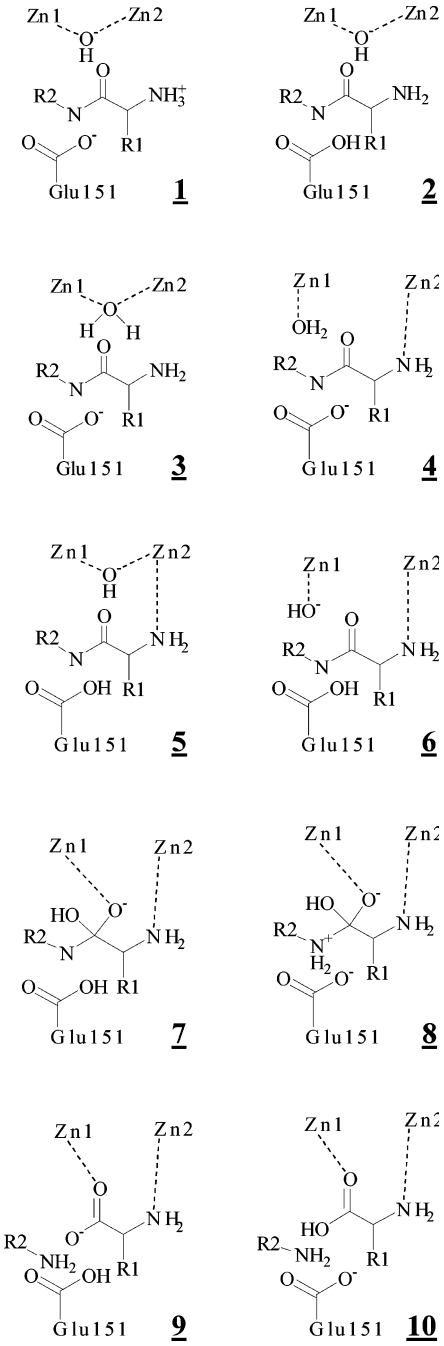

FIGURE 6: Notation of possible structures occurring during the catalytic reaction paths.

For a coordination to Zn2, the usually positively charged N-terminal amino group of the substrate must be deprotonated. The pK_a value of the amino group is usually about 8.0 (*49*), but it is likely that the interaction with the Zn^{2+} ion lowers it considerably. The deprotonation may occur in the solvent before the substrate enters the binding pocket or in the active site, where the bridging hydroxide ion or the carboxylate ligands Glu151 or Asp179 may act as proton acceptors. Because of the structural conditions, a deprotonation by Asp117 or Glu152 is unlikely. A major point of interest is the coordination pattern of the hydroxide/water−substrate complex. If the future nucleophile is a water molecule, it must be deprotonated to increase its nucleophi-

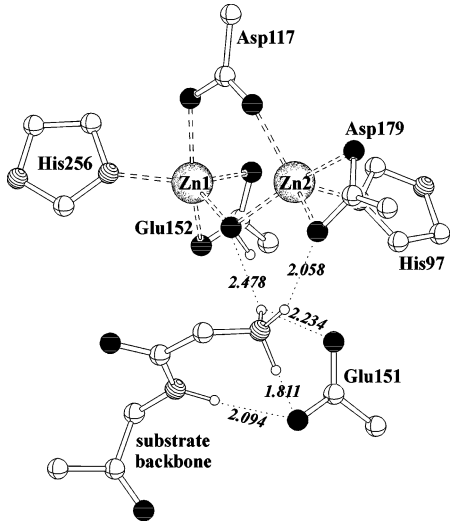

FIGURE 7: Active site with the protonated substrate (**1**) not yet coordinated to Zn2. Only the functional groups of the active site residues and essential protons are shown; the side chains of the substrate are omitted. The distances are given in Å.

licity. Again, Glu151 is an obvious candidate for the proton acceptor. The next step is the nucleophilic attack of the Zn^{2+}-bound hydroxide ion on the carbonyl carbon resulting in a tetrahedral intermediate. The open question concerning this reaction step is whether the hydroxide attacks from a bridging or a terminal position. For the decomposition of the tetrahedral intermediate, a proton must be transferred to the peptide nitrogen. A likely proton donor is Glu151 if it was protonated in an earlier step. However, the possibility of a proton transfer from the *gem*-diolate group to the peptide must also be considered. When the peptide cleavage is finished, the release of the N-terminal residue may only occur after a reprotonation of the amino group to facilitate its release from Zn2. Furthermore, possible interactions of the carboxyl or carboxylate group of the cleaved amino acid to the Zn^{2+} ions or other active site residues can also make product release difficult. However, the binding pocket is accessible to the solvent and an incoming water molecule can assist the cleavage of the products from the Zn^{2+} ions.

These various reaction possibilities were investigated and compared to determine the most likely. For clearness, the reaction steps are described individually. The discussion is confined to the reaction paths of the methyl-blocked Leu-Ala dipeptide via a tetrahedral intermediate in the *R*-configuration. Reaction paths via a tetrahedral intermediate in the *S*-configuration are not reported because only ones with unreasonably high activation energies were found.

Coordination of the Substrate to Zn2. Even if the substrate is not coordinated to Zn2 (**1**, see Figure 7), it is held in place by a number of hydrogen bonds. The protonated N-terminus interacts with both Glu151 carboxylate oxygens and with Asp179-Oδ2. Furthermore, Glu151-Oϵ2 is hydrogen-bonded to the peptide hydrogen of the scissile peptide bond. A very similar binding scheme was found in the X-ray structure for the leucine complex of the related *Streptomyces griseus* aminopeptidase (SGAP; PDB entry 1F2O; *50*).

For the deprotonation of the N-terminus, three proton acceptors are likely: Glu151, the hydroxide ion, and Asp179 (see Figure 8). The energies are given in Table 1 and the structure notation in Figure 6. The proton transfer to Glu151-Oϵ2 (path 1) has a very low activation barrier and is very exothermic. Subsequently, the N-terminal amino group can easily coordinate to Zn2 with a further gain in energy. This is by far the most favorable path for the binding step. The activation barrier for a proton transfer to the hydroxide ion (path 2) is 21.1 kcal mol^{-1}; to Asp179-Oδ2 (path 3), it is 26.7 kcal mol^{-1}. Path 3 was not followed further because of the high activation energy. The product of the hydroxide protonation in path 2 includes a bridging water molecule that takes up a terminal Zn1-coordinated position as soon as the N-terminus of the substrate is coordinated to Zn2 with virtually no activation barrier.

The results indicate that path 1 is the most likely, although the large gain in energy after the proton transfer to Glu151 is surprising. However, this reaction step calculated for the Cys227-Ser228-containing system has a slightly higher activation barrier (5.6 kcal mol^{-1}) and is less exothermic (−13.4 kcal mol^{-1}), indicating that Ser228 quenches the basicity of Glu151. The very low activation barrier for the coordination step in path 2 gives rise to the assumption that the proton transfer to the hydroxide ion, the coordination of the N-terminus, and the coordination cleavage of the water molecule to Zn2 may occur as a concerted process. In this case, a considerably lower activation energy may be required.

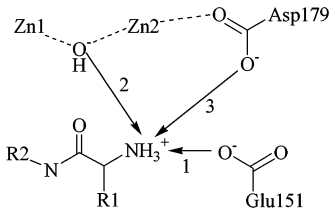

FIGURE 8: Possible proton acceptors for the deprotonation of the N-terminal ammonium group: (1) Glu151; (2) the hydroxide ion; (3) Asp179.

Table 1: Relative Energies (E), Activation Barriers (E_a), and Energy Differences from the Previous Minimum Structure (ΔE) in kcal mol^{-1} for the Coordination of the Substrate to the Zn^{2+} Ions (for the Notation of the Structures See Figure 6)[a]

structure	E	E_a	ΔE
(1) Proton Transfer to Glu151-Oϵ2 and Subsequent Coordination of the N-Terminus to Zn2			
1	0		
TS (H-transfer)	3.0	3.0	
2	−19.9		−19.9
TS (coordination)	−12.2	7.7	
5	−28.7		−8.8
(2) Proton Transfer to the Hydroxide Ion, Subsequent Coordination of the N-Terminus to Zn2, and Proton Transfer from the Water Molecule to Glu151			
1	0		
TS (H-transfer)	21.1	21.1	
3	10.9		10.9
TS (coordination)	11.2	0.3	
4	−7.1		−18.0
TS (H-transfer)	2.2	9.3	
6	−11.4		−4.3
(3) Proton Transfer to Asp179-Oδ2			
1	0		
TS (H-transfer)	26.7	26.7	
2′ (Asp179 instead of Glu151 protonated)	11.0		11.0

[a] A graphical representation is given in the Supporting Information (Figure S2).

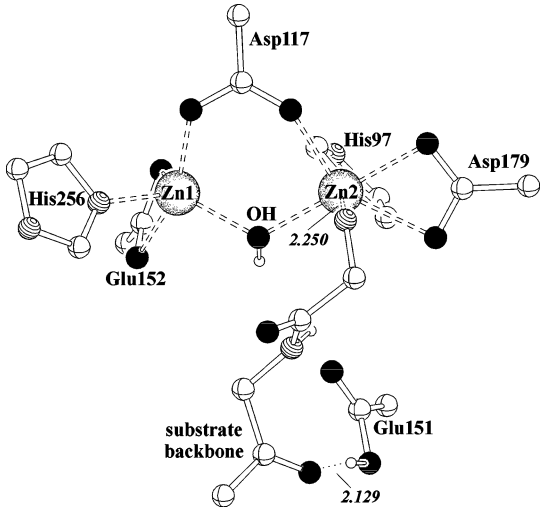

FIGURE 9: Enzyme−substrate complex including the bridging hydroxide ion (**5**). Only the functional groups of the active site residues and essential protons are shown; the side chains of the substrate are omitted. Distances are given in Å.

Although we did not find a corresponding transition state, this possibility should not be excluded. To regenerate the more nucleophilic hydroxide ion, the water can be deprotonated by Glu151. In the resulting structure **6**, the hydroxide ion is coordinated terminally to Zn1. This reaction step is exothermic.

To investigate the influence of the protonation state of Glu151, a further variant of path 2 with Glu151 protonated from the beginning was calculated. The proton transfer now requires an activation barrier of 14.3 kcal mol^{-1} and is only 1.3 kcal mol^{-1} exothermic. However, the protonated Glu151 forms a hydrogen bond to Asp179-Oδ2. As a consequence of the resulting electron deficiency on Zn2, the water molecule occupies the vacant binding position and inhibits the coordination of the N-terminal amino group to Zn2.

The conformation of the coordinated substrate **5** (see Figure 9) is stabilized by a hydrogen bond from Glu151-Hϵ2 to the C-terminal alanine carbonyl oxygen (H−O distance 2.129 Å). Depending on the conformation of the C-terminus, the total energy of this structure varies by up to 17 kcal mol^{-1}. Although the structure shown in Figure 9 was found to be the most stable, minimum structures without the Glu151-Hϵ2−Ala-O$_{CO}$ interaction are more appropriate for further reaction steps. This is justified because the extra stabilization of the most stable C-terminus conformation is a consequence of the attenuated substrate model. Larger protein substrates should not adopt this conformation. Partly, the C-terminus conformations are stabilized by hydrogen bonds between His256-Hϵ1 and the carbonyl oxygen of the scissile peptide bond or Ala-O$_{CO}$. The conformational changes are proposed to occur within the scope of the normal protein movement.

Nucleophilic Attack. The nucleophilic attack of the bridging hydroxide ion on the peptide carbonyl carbon requires an activation energy of 21.9 kcal mol^{-1} (path 1 in Table 2). However, an alternative and more favorable reaction possibility is the cleavage of the Zn2−hydroxide coordination and the attack of the resulting terminally bound hydroxide on the carbonyl carbon (path 2). For this path, the activation barriers are 12.4 kcal mol^{-1} for the breaking of the coordination and 17.0 kcal mol^{-1} for the nucleophilic attack.

Table 2: Relative Energies (E), Activation Barriers (E_a), and Energy Differences from the Previous Minimum Structure (ΔE) in kcal mol^{-1} for the Nucleophilic Attack (for the Notation of the Structures See Figure 6)[a]

stucture	E	E_a	ΔE
(1) Nucleophilic Attack of the Metal-Bridging Hydroxide Ion			
2	0		
TS (nucleophilic attack)	21.9	21.9	
7	10.1		10.1
(2) Cleavage of the Zn2 Coordination and Attack of the Terminal Hydroxide Ion			
2	0		
TS (coordination cleavage)	12.4	12.4	
6	6.1		6.1
TS (nucleophilic attack)	23.1	17.0	
7	10.1		4.0
(2a) Cleavage of the Zn2 Coordination			
2[b]	0		
TS[b] (coordination cleavage)	13.1	13.1	
6[b]	7.5		7.5

[a] A graphical representation is given in the Supporting Information (Figure S3). [b] Extended QM system including Asp99, Cys227, and Ser228.

We found the same situation for the formation of the tetrahedral intermediate in the blLAP, where the nucleophilic attack of a bridging hydroxide ion affords an about 10 kcal mol^{-1} higher activation energy than that of a terminally coordinated one (*1*). The structures of the terminal hydroxide complex **6** and the tetrahedral intermediate **7** are shown in Figure 10.

The terminal hydroxide in the structure **6** is stabilized by a hydrogen bond to the N-terminal amino group. As for **5**, a variety of minima depending on the starting structure for **6** were found. The most stable one shows the hydrogen bond between Glu151-Hϵ2 and Ala-O$_{CO}$ observed before in the most stable structure **5**. Furthermore, some conformers are stabilized by a weak interaction between the carbonyl oxygen of the scissile peptide bond and His256-Hϵ1. The structure shown in Figure 10a is more favorable for a nucleophilic attack than the most stable one. Because the activation energy of a Zn2−hydroxide coordination is only half as high as that for the coordination cleavage, the equilibrium lies on the **5** side and the terminal hydroxide complex **6** can be considered as an activated intermediate. Asp99 has been suggested to contribute to the regulation of the Zn2 Lewis acidity via His97. Thus, its influence on the bridging/terminal hydroxide complex equilibrium was studied on an extended model system including Asp99, Cys227, and Ser228 in the QM part (path 2a in Table 2). However, the activation barrier for the coordination cleavage is 0.7 kcal mol^{-1} higher and the relative energy of the terminal hydroxide complex is 1.4 kcal mol^{-1} higher, indicating that Asp99 slightly favors the bridging hydroxide complex.

The tetrahedral intermediate **7** is stabilized by the coordination of the *gem*-diolate group to Zn1 as a bidentate ligand and hydrogen bonds between the *gem*-diolate hydrogen and Glu151-Oϵ1 and between His256-Hϵ1 and the unprotonated *gem*-diolate oxygen. Furthermore, there is a hydrogen bond between Asp117-Oδ2 and the N-terminal amino group.

Decomposition of the Tetrahedral Intermediate. The following step in the hydrolysis reaction, the decomposition of the tetrahedral intermediate, requires the protonation of

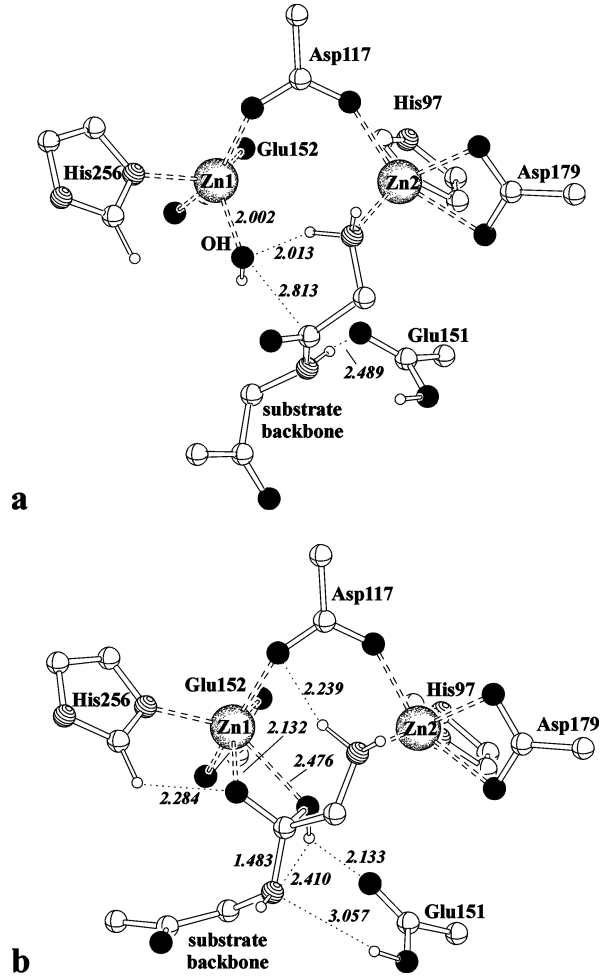

FIGURE 10: Enzyme−substrate complex (a) including the terminally coordinated hydroxide ion (**6**) and (b) with the tetrahedral intermediate (**7**). Only the functional groups of the active site residues and essential protons are shown; the side chains of the substrate are omitted. Distances are given in Å.

the former peptide nitrogen. The possible proton donors are the protonated Glu151 (path 1 in Figure 11) and the *gem*-diolate group (path 2).

The proton transfer from Glu151 results in a zwitterionic structure **8** that is stabilized by hydrogen bonds between Glu151-Oϵ2 and the peptide ammonium group and between Glu151-Oϵ2 and the *gem*-diolate hydrogen. The C−N bond is already elongated and is subsequently cleaved to form the product structure **10**. Now the coordinated leucine can for its part protonate Glu151 with a very low activation barrier leading to a negatively charged leucine, which is still coordinated to Zn1 via the carboxylate group and to Zn2 via the N-terminus. Structure **9** can also be obtained directly by a proton transfer from the *gem*-diolate group to Glu151 in structure **8** (path 3 in Figure 11). The transfer is accompanied by the cleavage of the C−N bond. The N-terminal end of the remaining peptide chain is hydrogen bonded via the amino nitrogen to His256-Hϵ1 or the carboxyl group of Glu151 and via one of the amino hydrogens to the leucine carboxylate oxygens. Although the release should be more difficult for a charged leucine, the low activation barrier suggests that structure **9**, rather than structure **10**, should be considered as the product of the chemical transformation. The structures 8 and 9 are shown in Figure 12; the relative energies of all decomposition possibilities are given in Table 3.

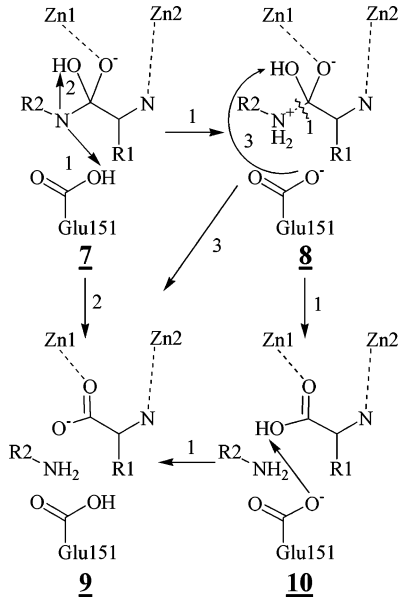

FIGURE 11: Possible paths for the decomposition of the tetrahedral intermediate **7** to the product structure **9**: (1) formation of the zwitterionic intermediate **8** via protonation of the peptide nitrogen by Glu151, subsequent cleavage of the C−N-bond resulting in **10**, and proton transfer from the leucine carboxyl group to Glu151; (2) protonation of the peptide nitrogen by the *gem*-diolate group; (3) decomposition of **8** by a proton transfer from *gem*-diolate group to Glu151.

The other alternative for the decomposition step is a proton transfer from the *gem*-diolate group to the peptide nitrogen (path 2). Simultaneously with the transfer reaction, the C−N-bond is broken, and **9** is formed. However, this possibility requires an activation energy nearly twice as high as that for the decomposition via **8**. The formation of the zwitterionic intermediate is the rate-determining step of the chemical reaction with an activation barrier of 26.9 kcal mol^{-1}. Although it is possible to mediate this proton transfer by a water molecule resulting in a hydronium ion as a very unstable additional intermediate, the activation barrier for this path is by 8.4 kcal mol^{-1} higher.

Coordination Cleavage of the Product to the Zn^{2+} Ions. The C-terminal fragment interacts with the active site residues only by hydrogen bonds, but the N-terminal leucine is much more tightly bound, especially if it is negatively charged. A neutral leucine is unlikely because it is calculated to be 26.1 kcal mol^{-1} less stable than the anion. Glu151 is the only available proton donor for the N-terminal amino group in **9**. However, a proton transfer is only possible if the coordination to Zn2 is detached first, which requires an activation energy of 14.8 kcal mol^{-1}. The subsequent proton transfer has an activation barrier of 22.0 kcal mol^{-1} and results in a leucine zwitterion that is still coordinated tightly to both Zn^{2+} ions via one carboxylate oxygen.

An additional water molecule added to the solvent-exposed active site improves the overall situation (the notation of the water-containing structures is given in Figure 13). Four possibilities for the formation of the structure **21** are theoretically possible (see Figure 14 and Table 4). The peptide fragments in structure **21** are not coordinated to the Zn^{2+} ions. The N-terminus of the leucine is positively

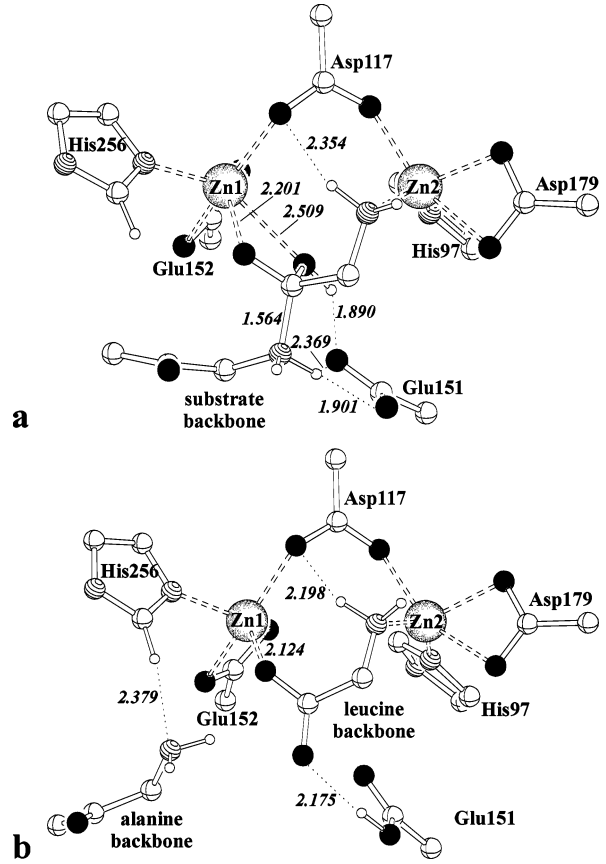

FIGURE 12: Complex (a) with the zwitterionic intermediate (**8**) and (b) product complex with a negatively charged leucine (**9**). Only the functional groups of the active site residues and essential protons are shown; the side chains of the substrate are omitted. Distances are given in Å.

charged, and the C-terminus is neutral. This protonation pattern ensures that the peptide does not coordinate to one of the Zn^{2+} ions and facilitates the product release. The active site is then ready for the next catalytic cycle. Nevertheless, it is not clear whether the N-terminal amino group must necessarily be protonated for the leucine to leave the binding pocket.

The additional water molecule is bound to Zn1 and occupies the coordination site of the leucine carboxyl or carboxylate oxygens, which are in return hydrogen-bonded to the water molecule. As a consequence, the stabilization of the negatively charged leucine by the Zn^{2+} ions decreases, as does the activation energy for the formation of a neutral leucine. Therefore, the proton transfer from the Glu151 carboxyl group in structure **11** (path 1 in Figure 14) now requires 12.5 kcal mol^{-1} and the return reaction 6.3 kcal mol^{-1}. Thus, a neutral leucine may be stable enough to leave the binding pocket. The additional water molecule is a potential donor for the protonation of the N-terminal amino group. However, again this must first be dissociated, which is the rate-limiting step for path 1 (see Figure 14). The resulting hydroxide ion is terminally bound to Zn1 and can take up the bridging position easily. The positively charged leucine in structure **21** interacts with the active site only by hydrogen bonds to Glu151, Asp179, and the hydroxide ion. In path 2, the release is initiated by a proton transfer from the water molecule to the leucine carboxyl group. The resulting hydroxide ion coordinates to Zn2 and facilitates

Table 3: Relative Energies (E), Activation Barriers (E_a), and Energy Differences from the Previous Minimum Structure (ΔE) in kcal mol^{-1} for the Decomposition of the Tetrahedral Intermediate (for the Notation of the Structures See Figure 6)[a]

structure	E	E_a	ΔE
(1) Proton Transfer from Glu151-Oϵ2 to the Peptide Nitrogen, C−N Bond Cleavage, and Proton Transfer from the Leucine Carboxyl Group to Glu151			
7	0		
TS (H-transfer to peptide N)	26.9	26.9	
8	20.9		20.9
TS (C−N bond cleavage)	31.5	10.6	
10	3.4		−17.4
TS (H-transfer to Glu151)	6.7	3.3	
9	−22.2		−26.7
(2) Proton Transfer from the *gem*-Diolate Group to the Peptide Nitrogen			
7	0		
TS (H-transfer to peptide N)	46.9	46.9	
9	−22.2		−22.2
(3) Proton Transfer from the *gem*-Diolate Group to Glu151-Oϵ1			
8	20.9		
TS (H-transfer to Glu151)	33.6	12.7	
9	−22.2		−43.1

[a] A graphical representation is given in the Supporting Information (Figure S4).

the cleavage of the Zn2−N-terminus coordination significantly. A subsequent proton transfer from Glu151 to the N-terminal amino group forming the target structure **21** is the rate-limiting step in path 2. In paths 3 and 4, the first step is the cleavage of the Zn2−N-terminus coordination, which is endothermic by 22.7 kcal mol^{-1}. However, we could not optimize a transition state for this system. Again, a possible support of the release by the His97-mediated interaction of Asp99 with Zn2 was studied by using the extended system including Asp99, Cys227, and Ser228 in the QM part. Now a transition state was found, and furthermore, the reaction step is 7.3 kcal mol^{-1} less endothermic than that in the smaller system. Although Asp99 was not found to have a significant effect on the Zn2−hydroxide coordination cleavage in **5**, it does influence the cleavage of the product from Zn2 by regulating the electronic conditions on Zn2. In path 3, a proton is transferred from the water molecule to the amino group with a very low activation energy, and the resulting hydroxide ion occupies a bridging position automatically to form system **19**. The final proton transfer from Glu151 to the leucine carboxylate group is rate-limiting. In path 4, the Glu151-Hϵ is transferred to the uncoordinated N-terminal amino group. Subsequently, the leucine carboxylate group is protonated by the water molecule, and the hydroxide ion coordinates to Zn2.

The results suggest strongly that the dissociation of the products from the Zn^{2+} ions must be assisted by a water molecule. The activation barriers of the rate-limiting steps for the various possibilities are similar, so it is likely that there is more than one reaction path. However, the final protonation of the amino group (which probably has a lower pK_a value than the usual pK_a of 8 because it interacts with Zn2 and thus may not be protonated within the active site) in path 2 or of the leucine carboxylate group in path 3 may not be necessary or may be assisted by the solvent. In both cases, the proton donor is Glu151. The remarkable basicity of this residue in its negatively charged form must be

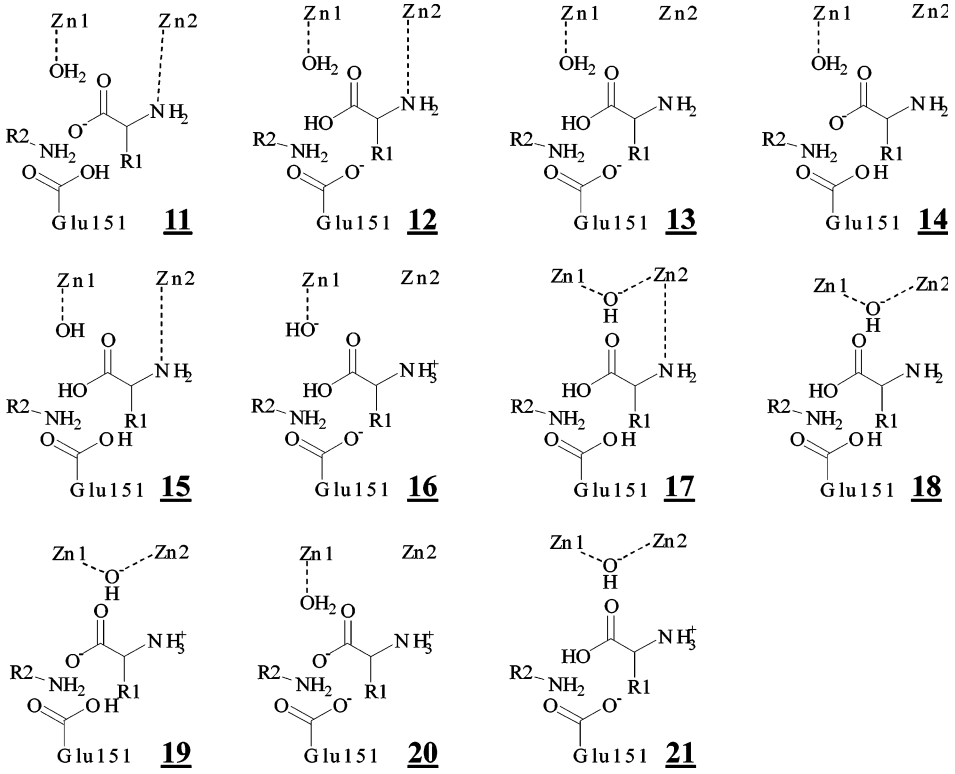

FIGURE 13: Notation of structures (including an additional water molecule) occurring during the possible product release processes.

quenched by additional solvent water molecules. As a consequence, the activation barriers for proton-transfer reactions with Glu151 as the donor should be lowered.

Electrostatic Effects. In the classical picture of enzyme catalysis, the electrostatic effect of the enzyme environment is suggested to make the largest contribution favoring the catalytic reaction (*51*). A dielectric constant of $\epsilon = 4$ was used for all calculations described above.

However, we can assume that the influence of the solvent for the monomeric AAP may not be described adequately, because the interactions between polar groups across the QM/MM boundary do not take the back-polarization of the MM part by the QM part into account. A better description requires the inclusion of a water cap in the QM part of the system or the use of a polarizable continuum model instead of the MM environment. Therefore, single point calculations of the QM part were performed using COSMO (*52*) with a dielectric constant of 78.54 for water as solvent. The shape of the QM system including a large part of the active site ensures that the major effect of the continuum affects the substrate at the solvent-exposed side and the enzyme-oriented side is shielded by the active site residues. A comparison of the energy profiles is shown in Figure 15.

The continuum has a stabilizing influence on the transition state of the rate-limiting formation of the zwitterionic intermediate **8**; the activation barrier is lowered significantly (by 7.1 kcal mol^{-1}). With the exception of the proton transfer to Glu151 in structure **10**, the barriers for the other reaction steps are also lowered slightly. Furthermore, the large energy changes found for the decomposition of the zwitterionic intermediate using the QM/MM method are quenched by the effect of the polarizable continuum. To prove whether the enzyme environment catalyzes the chemical transformation at all, single point energies within a COSMO polarizable continuum on reduced substrate structures were performed (see Figure 15). These systems contain the dipeptide, Glu151, which is represented by an acetate ion, and the two Zn^{2+} ions with a coordination shell of three water molecules each. To describe a more realistic picture, the water molecules were allowed to relax while the rest of the system was frozen to the conformation obtained by the QM/MM calculation. The resulting energy profile agrees very well with the conclusions that we have drawn from the calculations with the enzyme and continuum environment. The rate-limiting formation of the zwitterionic intermediate **8** is more favorable in solvent, emphasizing its importance for this step. All other reaction steps are favored by the enzyme active site residues and environment. The relative energies are listed in Table 5.

Energetic Comparison of the Semiempirical Calculations to DFT. To confirm the reaction mechanism obtained by the semiempirical method, we calculated the PW91/DNP (*41*, *43*) energies for the QM/MM stationary points along the reaction path. Figure 16 shows the comparison between the DFT energies and AM1 gas-phase single point energies on the same systems.

The agreement of the relative energies between the two methods for the structures **5**, **10**, and **9** is as expected and found previously for the blLAP. The energies of the terminal hydroxide complex **6** and the transition state for the nucleophilic attack are probably underestimated and the transition states for the proton-transfer reactions and the energy of the zwitterionic intermediate **8** overestimated by AM1. The DFT profile for the decomposition of the tetrahedral intermediate suggests that the zwitterionic intermediate may be an artifact of the method and that the proton transfer and the bond cleavage are concerted reactions, as similar calculations also suggested for the blLAP (*1*). Furthermore, the DFT calculations support the hypothesis that a neutral leucine as a product

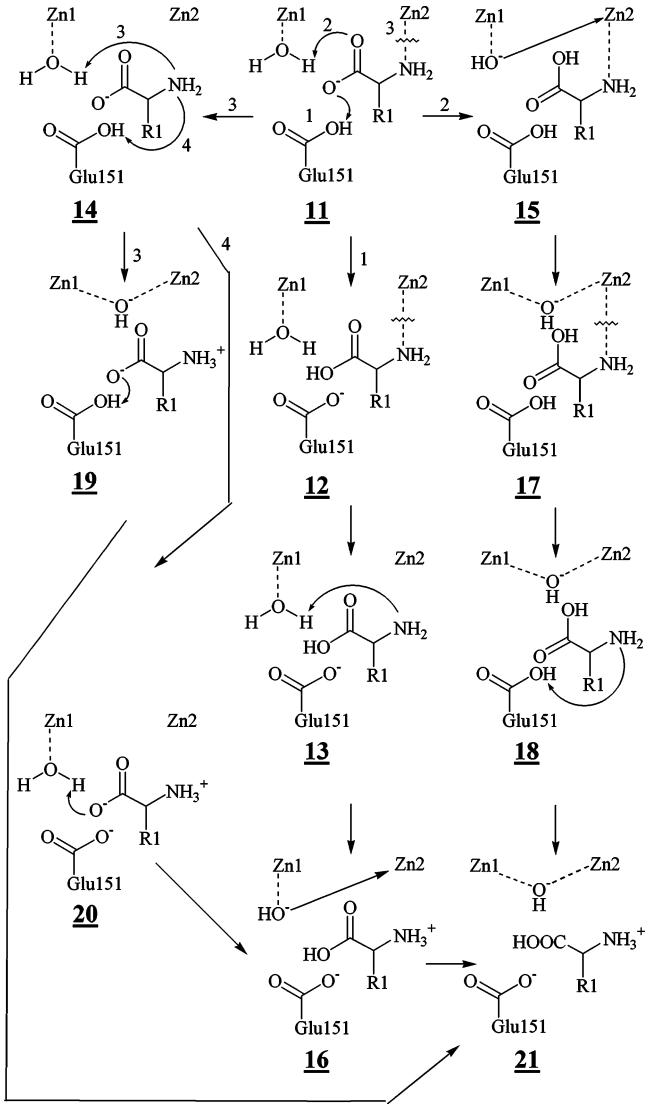

FIGURE 14: Possibilities for the water-assisted dissociation of the products from the zinc ions: (1) protonation of the leucine carboxylate group by Glu151, Zn2−N coordination cleavage, protonation of the N-terminus by the water, and Zn2 coordination of the hydroxide ion; (2) protonation of the leucine carboxylate group by the water, Zn2 coordination of the hydroxide ion, Zn2−N coordination cleavage, and protonation of the N-terminus by Glu151; (3) Zn2−N coordination cleavage, protonation of the N-terminus by the water (the Zn2 coordination of the hydroxide ion takes place automatically), and protonation of the leucine carboxylate group by Glu151; (4) Zn2−N coordination cleavage as in path 3, protonation of the N-terminus by Glu151, protonation of the leucine carboxylate group by the water, and Zn2 coordination of the hydroxide ion.

Table 4: Relative Energies (E), Activation Barriers (E_a), and Energy Differences from the Previous Minimum Structure (ΔE) in kcal mol^{-1} for the Water-Assisted Dissociation of the Products from the Zn^{2+} Ions (for the Notation of the Structures See Figure 13)[a]

structure	E	E_a	ΔE
(1) Protonation of the Leucine Carboxylate Group by Glu151, Cleavage of the Zn2−N-Terminus Coordination, Proton Transfer from the Water Molecule to the Amino Group, and Coordination of the Hydroxide Ion to Zn2			
11	0		
TS (H-transfer)	12.5	12.5	
12	6.2		6.2
TS (coordination cleavage)	26.0	19.8	
13	25.9		19.7
TS (H-transfer)	38.4	12.5	
16	31.8		5.9
TS (coordination)	33.3	1.5	
21	15.4		−16.4
(2) Proton Transfer from the Water Molecule to the Leucine Carboxylate Group, Hydroxide Coordination to Zn2, Zn2−N-Terminus Coordination Cleavage, and Protonation of the Amino Group by Glu151			
11	0		
TS (H-transfer)	15.4	15.4	
15	4.5		4.5
TS (coordination)	11.8	7.3	
17	2.2		−2.3
TS (coordination cleavage)	5.6	3.4	
18	−5.8		−8.0
TS (H-transfer)	16.9	22.7	
21	16.6		22.4
(3) Cleavage of the Zn2−N-Terminus Coordination, Proton Transfer from the Water Molecule to the Amino Group (the Coordination of the Hydroxide Ion to Zn2 Takes Place Automatically), and Protonation of the Leucine Carboxylate Group by Glu151			
11[b]	0		
TS[b] (coordination cleavage)	18.2	18.2	
14[b]	15.4		15.4
TS (H-transfer)	18.4	3.0	
19	4.4		−11.0
TS (H-transfer)	24.0	19.6	
21	2.5		−1.9
(4) Proton Transfer from Glu151 to the Amino Group, Protonation of the Leucine Carboxylate by the Water Molecule, and Coordination of the Hydroxide Ion to Zn2			
14	15.4		
TS (H-transfer)	37.7	22.3	
20	29.0		13.6
TS (H-transfer)	39.8	10.8	
16	33.3		4.3
TS (coordination)	36.1	2.8	
21	23.5		−9.8

[a] A graphical representation is given in the Supporting Information (Figure S5). [b] Extended QM system including Asp99, Cys227, and Ser228.

is not likely. Overall, the AM1 calculations give a good qualitative description. However, we have noted previously (*53*) that the balance between Zn−N and Zn−O coordination is extremely difficult to reproduce with either DFT or semiempirical methods, so systematic errors in our energies may result from this source. The tendency of AM1 and DFT to over- and underestimate proton-transfer barriers, respectively, is evident from our results.

DISCUSSION

The results of the QM/MM study confirm the mechanism proposed by Stamper et al. (*14*) to a high degree. After the coordination of the N-terminal amino group to Zn2, the bridging hydroxide ion becomes terminally bound to Zn1 and, although there is probably an equilibrium between the structures **6** and **5** with the latter favored, attacks the peptide carbonyl carbon out of this position. Our earlier study on blLAP (*1*) revealed the same situation. The terminally bound hydroxide complex can be regarded as an activated intermediate. Recently, on the basis of molecular dynamics simulations, Merz et al. suggested a similar breaking of a hydroxide bridge to facilitate the nucleophilic attack for the binuclear zinc−β-lactamase of *Bacteroides fragilis* complexed with imipenem (*54*). As in our earlier blLAP study and in contrast to the mechanism proposed by Stamper et al., the substrate carbonyl oxygen in the structures **6** and **5** is not coordinated to Zn1. The substrate is merely held in

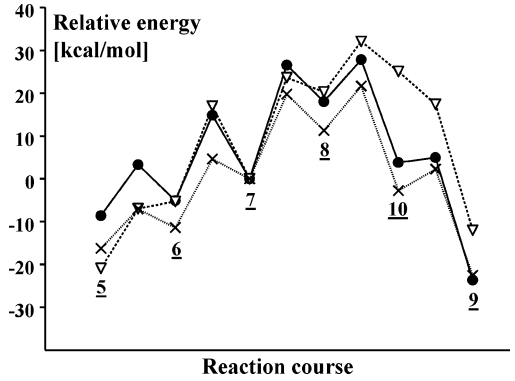

FIGURE 15: Comparison of the energy profiles obtained with the MM environment AAP directly generated from the PDB entry 1FT7 ($\epsilon = 4$, —, ●), with a COSMO continuum model instead of the MM environment ($\epsilon = 78.54$, ···, ×), and with a model system containing the substrate and the two Zn^{2+} ions with three water molecules each within a COSMO continuum model ($\epsilon = 78.54$, − − −, ▽). The water molecules were optimized, while the rest of the system was frozen in the conformation obtained by the QM/MM calculations.

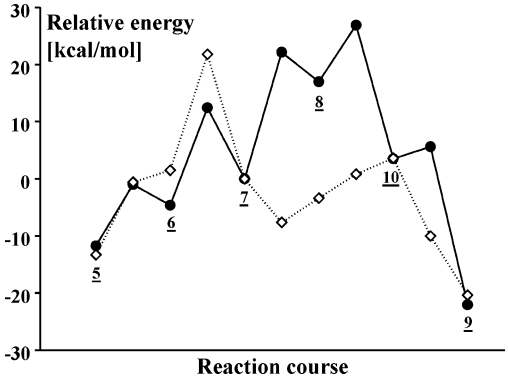

FIGURE 16: Comparison between AM1 (—, ●) and PW91/DNP (− − −, ◇) gas-phase single point energies on the stationary points of the reaction path.

place by hydrogen bonds to Glu151 or His256. The nucleophilic attack is accompanied by the coordination of the carbonyl oxygen to Zn1. The resulting tetrahedral intermediate is stabilized by interactions of the two *gem*-diolate oxygens to Zn1, but conformations with similar energy were also found with only the unprotonated oxygen coordinated to the metal ion or with an additional interaction of the protonated oxygen to Zn2. In agreement with Stamper et al., the donor for the subsequent protonation of the peptide nitrogen is Glu151, which was protonated in an earlier step. The breaking of the peptide bond and a proton transfer from the *gem*-diolate group or leucine carboxyl group, respectively, finish the chemical transformation. As suggested in the literature, we found the decomposition of the tetrahedral intermediate by the proton transfer from Glu151 to the peptide nitrogen to be the rate-limiting step.

A minor difference from the literature is the importance of the Asp99−His97−Zn2 triad. Stamper et al. suggest that it contributes to the regulation of the Lewis acidity of Zn2 and assists the breaking of the hydroxide bridge in this way. We cannot confirm an effect on this reaction step, but the triad clearly has an influence on the coordination cleavage of the product to Zn2. However, a look on the topology shows that the position of Asp99-Oδ1 is not ideal because it is not in plane with the His97 imidazole ring. The dihedral angle describing the aspartate−histidine orientation (Asp99-Oδ1, His97-Nδ1, His97-Cϵ1, His97-Nϵ2) ranges from 128° in the PDB entry 1IGB to 146° in 1CP6. Christianson et al. examined carboxylate−histidine−zinc interactions in protein structures (*21*). The average value of the corresponding dihedral of seven protein structures is 169° as given in the publication and 176° taking into account that the PDB entry 1CAC, which was the by far worst outlier, has meanwhile been superseded by 1CA2. The aspartate−histidine interaction is therefore not optimal in AAP, and thus, the impact on Zn2 is lower than expected.

The negatively charged Glu151 shows enhanced basicity compared to the free amino acid. The corresponding acid has a pK_a value of about 4.4 (*49*), so a glutamate residue is expected not to be protonated at physiological pH. However, the low activation barriers for proton-transfer reactions to

Table 5: Relative Energies (E), Activation Barriers (E_a), and Energy Differences from the Previous Minimum Structure (ΔE) in kcal mol^{-1} of the Most Likely Reaction Path with Different Environments[a]

	AAP			AAP(cosmo)			solvent(cosmo)		
structure	E	E_a	ΔE	E	E_a	ΔE	E	E_a	ΔE
2	−10.1			−16.3			−20.9		
TS (coordination cleavage)	2.2	12.3		−7.1	9.2		−7.0	13.9	
6	−4.0		6.1	−11.4		4.9	−5.3		15.6
TS (nucleophilic attack)	13.0	17.0		4.6	16.0		17.0	24.0	
7	0.0		4.0	0.0		11.4	0.0		5.3
TS (H-transfer to peptide N)	26.9	26.9		19.8	19.8		23.6	23.6	
8	20.9		20.9	11.3		11.3	20.3		20.3
TS (C−N bond cleavage)	31.5	10.6		21.7	10.4		32.1	11.8	
10	3.5		−17.4	−2.8		−14.1	25.1		4.8
TS (H-transfer to Glu151)	6.7	3.2		2.3	5.1		17.4	−7.7	
9	−22.2		−25.7	−22.6		−19.8	−12.0		−37.1

[a] AAP, The MM environment AAP directly generated from the PDB entry 1FT7 ($\epsilon = 4$); AAP(cosmo), a COSMO continuum model instead of the MM environment ($\epsilon = 78.54$); solvent(cosmo), a reduced model system containing the substrate and the two Zn^{2+} ions with three water molecules each within a COSMO continuum model ($\epsilon = 78.54$). For AAP(cosmo) and solvent(cosmo) single point calculations on the stationary points obtained with the AAP environment were performed. Please note that the values E_a and ΔE in the COSMO models have no physical meaning because the geometries are not necessarily minima or transition states and are only given for comparison. For AAP, the total energies are given; for AAP(cosmo) and solvent(cosmo), the heat of formation is given (for the notation of the structures, see Figure 6).

Glu151, the rather high barriers for transfers from this residue, and the stability of the structures with Glu151 protonated (e.g., **9**) indicate that its actual pK_a value is considerably higher. In the X-ray structures of the free enzyme (PDB entry 1AM) and the complex with 1-butaneboronic acid (1CP6), a water molecule is positioned closely to Glu151-Oϵ2. In the Zn^{2+}-coordinated inhibitor containing structures 1IGB and 1FT7, Glu151 interacts with the inhibitor via hydrogen bond donation. Calculations on a model system including Ser228, which is hydrogen-bonded to Glu151 in the geometry-optimized structures, indicate that the serine has a modulating influence on the glutamate basicity. Moreover, the AAP active site is solvent-exposed to a high degree, and a negatively charged Glu151 can be hydrated by water molecules immediately. Therefore, the basicity is probably overestimated but nonetheless higher than that of the free amino acid making Glu151 suitable as the general base.

Despite the differences in the mechanistical proposals for the blLAP (*28*, *9*) and the AAP (*14*) in the literature, we found many analogies to our earlier study on the mode of action of blLAP in the AAP reaction mechanism. Both enzymes prefer a reaction via the *R*-configuration of the tetrahedral intermediate. The nucleophilic attack of the hydroxide ion occurs from a terminally Zn1- (AAP) or Zn488-coordinated (blLAP) position and is accompanied by the formation of a substrate carbonyl oxygen−zinc coordination. The overall shape of the energy profile is very similar, and the rate-determining step was found to be the decomposition of the tetrahedral intermediate in the two enzymes. The role of the general base, Glu151 in the AAP, is taken over by Lys262 in the blLAP. The functions of the Zn^{2+} ions are also similar: Zn1 in the AAP, which corresponds to Zn488 in the blLAP, binds and stabilizes the nucleophilic hydroxide ion and the *gem*-diolate group of the tetrahedral intermediate; Zn2 (Zn489 in blLAP) binds the N-terminal amino group of the substrate.

Considering the good agreement of our results with the mechanism proposed by Stamper et al. (*14*) and the conclusions drawn from experiments (*16*−*20*), we suggest that the QM/MM approach using the AM1 Hamiltonian gives a good qualitative description of the catalytic mechanism of the AAP. Especially the confirmation of the results with various techniques such as DFT and COSMO energy calculations makes the overall picture reliable. However, the QM/MM approach investigates merely the potential surface of the static system and, thus, neglects any dynamical effects. Advanced calculations should include molecular dynamics averaging to take the conformational movements of the protein into account. (*32*) Moreover, a more quantitative examination of the catalytic process requires free energy calculations, for example, by using the EVB method (*33*). Both of these aspects, however, go beyond the scope of this work, of which the intention is to give a qualitative picture by comparing the various reaction possibilities.

The mode of action found for the AAP corresponds to a high degree to that found for the blLAP. This and the fact that one feature, the attack of a terminally coordinated hydroxide, was also suggested for the metallo-β-lactamase by Merz et al. (*54*) support the hypothesis that the mode of action of binuclear zinc hydrolases is, at least partly, based on a common reaction mechanism.

ACKNOWLEDGMENT

The authors thank Anselm Horn for programming support.

SUPPORTING INFORMATION AVAILABLE

A schematic representation of the system separation procedure (Figure S1), structural details of the optimized LPA−AAP systems (Table S1), and the graphical representations of Tables 1−4 (Figures S2−S5). This material is available free of charge via the Internet at http://pubs.acs.org.

REFERENCES

1. Schürer, G., Horn, A. H. C., Gedeck, P., and Clark, T. (2002) The Reaction Mechanism of Bovine Lens Leucine Aminopeptidase, *J. Phys. Chem. B 106*, 8815−8830.
2. (a) Taylor, A. (1993) Aminopeptidases: Structure and Function, *FASEB J. 7*, 290−298. (b) Taylor, A. (1993) Aminopeptidases: Towards a Mechanism of Action, *Trends Biochem. Sci. 18*, 167−172.
3. Pulido-Cejudo, G., Conway, B., Proulx, P., Brown, R., and Izaguirre, C. A. (1997) Bestatin-Mediated Inhibition of Leucine Aminopeptidase May Hinder HIV Infection, *Antiviral Res. 36*, 167−177.
4. Gonzales, T., and Robert-Baudouy, J. (1996) Bacterial Aminopeptidases: Properties and Functions, *FEMS Microbiol. Rev. 18*, 319−344.
5. Review on zinc enzymology: Lipscomb, W. N., and Sträter, N. (1996) Recent Advances in Zinc Enzymology, *Chem. Rev. 96*, 2375−2433.
6. Roderick, S. L., and Matthews, B. W. (1993) Structure of the Cobalt-Dependent Methionine Aminopeptidase from *Escherichia coli*: A New Type of Proteolytic Enzyme, *Biochemistry 32*, 3907−3912.
7. Sträter, N., Sherratt, D. J., and Colloms, S. D. (1999) X-ray structure of Aminopeptidase A from *Escherichia coli* and a Model for the Nucleoprotein Complex in Xer Site-Specific Recombination, *EMBO J. 18*, 4513−4522.
8. (a) Wilcox, D. E. (1996) Binuclear Metallohydrolases, *Chem. Rev. 96*, 2435−2458. (b) Sträter, N., Lipscomb, W. N., Klabunde, T., and Krebs, B. (1996) Two-Metal Ion Catalysis in Enzymatic Acyl- and Phosphoryl-Transfer Reactions, *Angew. Chem., Int. Ed. Engl. 35*, 2024−2055.
9. Sträter, N., Sun, L., Kantrowitz, E. R., and Lipscomb, W. N (1999) A Bicarbonate Ion as a General Base in the Mechanism of Peptide Hydrolysis by Dizinc Leucine Aminopeptidase, *Proc. Natl. Acad. Sci. U.S.A. 96*, 11151−11155.
10. Berman, H. M., Westbrook, J., Feng, Z., Gilliland, G., Bhat, T. N., Weissig, H., Shindyalov, I. N., and Bourne, P. E. (2000) The Protein Data Bank, *Nucleic Acids Res. 28*, 235−242.
11. Chevrier, B., Schalk, C., D'Orchymont, H., Rondeau, J.-M., Moras, D., and Tarnus, C. (1994) Crystal Structure of *Aeromonas proteolytica* Aminopeptidase: A Prototypical Member of the Co-Catalytic Zinc Enzyme Family, *Structure 2*, 283−291.
12. Chevrier, B., D'Orchymont, H., Schalk, C., Tarnus, C., and Moras, D. (1996) The Structure of the *Aeromonas proteolytica* Aminopeptidase Complexed with a Hydroxamate Inhibitor, *Eur. J. Biochem. 237*, 393−398.
13. De Paola, C. C., Bennett, B., Holz, R. C., Ringe, D., and Petsko, G. A. (1999) 1-Butaneboronic Acid Binding to *Aeromonas proteolytica* Aminopeptidase: A Case of Arrested Development, *Biochemistry 38*, 9048−9053.
14. Stamper, C., Bennett, B., Edwards, T., Holz, R. C., Ringe, D., and Petsko, G. (2001) Inhibition or the Aminopeptidase from *Aeromonas proteolytica* by L-Leucinephosphonic acid. Spectroscopic and Crystallographic Characterization of the Transition State of Peptide Hydrolysis, *Biochemistry 40*, 7035−7046.
15. Christianson, D. W. (1991) Structural Biology of Zinc, *Adv. Protein Chem. 42*, 281−355.
16. Chen, G., Edwards, T., D'souza, V. M., and Holz, R. C. (1997) Mechanistic Studies on the Aminopeptidase from *Aeromonas proteolytica*: A Two-Metal Ion Mechanism for Peptide Hydrolysis, *Biochemistry 36*, 4278−4286.
17. Bennett, B., and Holz, R. C. (1997) EPR Studies on the Mono- and Dicobalt(II)-Substituted Forms of the Aminopeptidase from

Aeromonas proteolytica. Insight into the Catalytic Mechanism of Dinuclear Hydrolases, *J. Am. Chem. Soc. 119*, 1923−1933.
18. Bennett, B., and Holz, R. C. (1997) Spectroscopically Distinct Cobalt(II) Sites in Heterodimetallic Forms of the Aminopeptidase from *Aeromonas proteolytica*: Characterization of Substrate Binding, *Biochemistry 36*, 9837−9846.
19. Holz, R. C., Bennett, B., Chen, G., and Ming, L.-J. (1998) Proton NMR Spectroscopy as a Probe of Dinuclear Copper(II) Active Sites in Metalloproteins. Characterization of the Hyperactive Copper(II)-Substituted Aminopeptidase from *Aeromonas proteolytica*, *J. Am. Chem. Soc. 120*, 6369−6335.
20. Bennett, B., and Holz, R. C. (1998) Inhibition of the Aminopeptidase from *Aeromonas proteolytica* by L-Leucinephosphonic Acid, a Transition State Analogue of Peptide Hydrolysis, *J. Am. Chem. Soc. 120*, 12139−12140.
21. Christianson, D. W., and Alexander, R. S. (1989) Carboxylate−Histidine−Zinc Interactions in Protein Structure and Function, *J. Am. Chem. Soc. 111*, 6412−6419.
22. Ustynyuk, L., Bennett, B., Edwards, T., and Holz, R. C. (1999) Inhibition of the Aminopeptidase from *Aeromonas proteolytica* by Aliphatic Alcohols. Characterization of the Hydrophobic Substrate Recognition Site, *Biochemistry 38*, 11433−11439.
23. Huntington, K. M., Bienvenue, D. L., Wei, Y., Bennett, B., Holz, R. C., and Pei, D. (1999) Slow-Binding Inhibition of the Aminopeptidase from *Aeromonas proteolytica* by Peptide Thiols: Synthesis and Spectroscopic Characterization, *Biochemistry 38*, 15587−15596.
24. Bienvenue, D. L., Bennett, B., and Holz, R. C. (2000) Inhibition of the Aminopeptidase from *Aeromonas proteolytica* by L-Leucinethiol: Kinetic and Spectroscopic Characterization of a Slow, Tight-Binding Inhibitor-Enzyme Complex, *J. Inorg. Chem. 78*, 43−54.
25. Bienvenue, D. L., Gilner, D., and Holz, R. C. (2002) Hydrolysis of Thionopeptides by the Aminopeptidase from *Aeromonas proteolytica*: Insight into Substrate Binding, *Biochemistry 41*, 3712−3719.
26. Kim, H., and Lipscomb, W. N. (1993) Differentiation and Identification of the Two Catalytic Metal Binding Sites in Bovine Lens Leucine Aminopeptidase by X-ray Crystallography, *Proc. Natl. Acad. Sci. U.S.A 90*, 5006−5010.
27. Burley, S. K., David, P. R., Taylor, A., and Lipscomb, W. N. (1990) Molecular Structure of Leucine Aminopeptidase at 2.7 Å Resolution, *Proc. Natl. Acad. Sci. U.S.A. 87*, 6878−6882.
28. Sträter, N., and Lipscomb, W. R. (1995) Transition State Analogue L-Leucinephosphonic Acid Bound to Bovine Lens Leucine Aminopeptidase: X-ray Structure at 1.65 Å Resolution in a New Crystal Form, *Biochemistry 34*, 9200−9210.
29. Warshel, A., and Levitt, M. (1976) Theoretical studies of enzymic reactions: dielectric, electrostatic and steric stabilization of the carbonium ion in the reaction of lysozyme, *J. Mol. Biol. 103*, 227−249.
30. Some examples: (a) Schmidt, R. K., and Gready, J. E. (2000) Conformational Preferences of the Substrates of Lactate Dehydrogenase, *J. Mol. Struct. (THEOCHEM) 498*, 101−112. (b) Martí, S., Andrés, J., Moliner, V., Silla, E., Tuñón, I., and Bertrán, J. (2000) A QM/MM Study of the Conformational Equilibria in the Chorismate Mutase Active Site. The Role of the Enzymatic Deformation Energy Contribution, *J. Phys. Chem. B 104*, 11308−11315. (c) Titmuss, S. J., Cummins, P. L., Bliznyuk, A. A., Rendell, A. P., and Gready, J. E. (2000) Comparison of Linear-Scaling Semiempirical Methods and Combined Quantum Mechanical/Molecular Mechanical Methods Applied to Enzyme Reactions, *Chem. Phys. Lett. 320*, 169−176. (d) Antonczak, S., Monard, G., Ruiz-Lopez, M. F., and Rivail, J.-L. (1998) Modeling of Peptide Hydrolysis by Thermolysin. A Semiempirical and QM/MM Study, *J. Am. Chem. Soc. 120*, 8825−8833. (e) Hart, J. C., Burton, N. A., Hillier, I. H., Harrison, M. J., and Jewsbury, P. (1997) Prediction of Transition State Structure in Protein Tyrosine Phosphatase Catalysis Using a Hybrid QM/MM Potential, *Chem. Commun.* 1431−1432. (f) Cunningham, M. A., Ho, L. L., Nguyen, D. T., Gillilan, R. E., and Bash, P. A. (1997) Simulation of the Enzyme Reaction Mechanism of Malate Dehydrogenase, *Biochemistry 36*, 4800−4816. (g) Lyne, P. D., Mulholland, A. J., and Richards, W. G. (1995) Insights into Chorismate Mutase Catalysis from a Combined QM/MM Simulation of the Enzyme Reaction, *J. Am. Chem. Soc. 117*, 11345−11350.
31. Antonczak, S., Ruiz-López, M., and Rivail, J.-L. (1997) The Hydrolysis Mechanism of Formamide Revisited: Comparison Between ab initio, Semiempirical and DFT Results, *J. Mol. Model. 3*, 434−442.
32. Warshel, A. (2003) Computer simulations of enzyme catalysis: Methods, progress, and insights, *Annu. Rev. Biophys. Biomol. Struct. 32*, 425−443.
33. Warshel, A., and Weiss, R. M. (1980) *J. Am. Chem. Soc. 102*, 6218−6226.
34. Clark, T., Alex, A., Beck, B., Chandrasekhar, J., Gedeck, P., Horn, A., Hutter, M., Martin, B., Rauhut, G., Sauer, W., Schindler, T., and Steinke, T. *Vamp 7.5*; Computer-Chemie-Centrum, Universitaet Erlangen-Nuremberg: Erlangen-Nürnberg, 2001.
35. Clark, M., Cramer, R. D., III, and Van Opdenbosch, N. (1989) Validation of the General Purpose Tripos 5.2 Force Field, *J. Comput. Chem. 10*, 982−1012.
36. *Sybyl 6.6*, Tripos Associates: St. Louis, MO, 1999.
37. Dewar, M. J. S., Zoebisch, E. G., Healy, E. F., and Stewart, J. J. P. (1985) Development and Use of Quantum Mechanical Molecular Models. 76. AM1: A New General Purpose Quantum Mechanical Molecular Model, *J. Am. Chem. Soc. 107*, 3902−3909.
38. Dewar, M. J. S., and Merz, K. M., Jr. (1988) AM1 Parameters for Zinc, *Organometallics 7*, 522−524.
39. (a) Liu, D. C., and Nocedal, J. (1985) On the Limited Memory Method for Large Scale Optimization, *Math. Programming 45*, 503−528. (b) Nocedal, J. (1980) Updating Quasi-Newton Matrices with Limited Storage, *Math. Comput. 24*, 773−782.
40. (a) Banerjee, A., Adams, N., Simons, J., and Shepard, R. (1985) Search for Stationary Points on Surfaces, *J. Phys. Chem. 89*, 52−57. (b) Baker, J. (1986) An Algorithm for the Location of Transition States, *J. Comput. Chem. 7*, 385−395.
41. (a) Delley, B. (1990) An All-Electron Numerical Method for Solving the Local Density Functional for Polyatomic Molecules, *J. Chem. Phys. 92*, 508−517. (b) Delley, B. (2000) From Molecules to Solids with the $DMol^3$ Approach, *J. Chem. Phys. 113*, 7756−7764.
42. *Materials Studio 2.1.5*; Accelrys Inc.: San Diego, CA, 2002.
43. Perdew, J. P., and Wang, Y. (1992) Accurate and Simple Analytic Representation of the Electron-Gas Correlation Energy, *Phys. Rev. B 45*, 13244−13249.
44. Wesolowski, T. A., Parisel, O., Ellinger, Y., and Weber, J. (1997) A Comparative Study of Benzene···X (X = O_2, N_2, CO) Complexes using Density Functional Theory: The Importance of an Accurate Exchange−Correlation Energy Density at High Reduced Density Gradients, *J. Phys. Chem. A 101*, 7818−7825.
45. Schürer, G., Lanig, H., and Clark, T. (2000) The Mode of Action of Phospholipase A_2: Semiempirical MO Calculations Including the Protein Environment, *J. Phys. Chem. B 104*, 1349−1361.
46. Gasteiger, J., and Marsili, M. (1980) Iterative Partial Equalization of Orbital Electronegativity − A Rapid Access to Atomic Charges, *Tetrahedron 36*, 3219−3228.
47. Holleman, A. F., and Wiberg, E. (1985) *Lehrbuch der Anorganischen Chemie*, 91.-100. Ausgabe, p 651, Walter de Gruyter, Berlin.
48. Zheng, Y. J., and Merz, K. M., Jr. (1992) Study of Hydrogen Bonding Interactions Relevant to Biomolecular Structure and Function, *J. Comput. Chem. 13*, 1151−1169.
49. Stryer, L. (1999) *Biochemie*, 4. Auflage, p 22, Spektrum Akademischer Verlag, Heidelberg, Germany.
50. Gilboa, R., Spungin-Bialik, A., Wohlfahrt, G., Schomburg, D., Blumberg, S., and Shoham, G. (2001) Interactions of *Streptomyces griseus* Aminopeptidase With Amino Acid Reaction Products and Their Implications Toward a Catalytic Mechanism, *Proteins: Struct., Funct., Genet. 44*, 490−504.
51. Warshel, A., and Åqvist, J. (1991) Electrostatic Energy and Macromolecular Function, *Annu. Rev. Biophys. Biophys. Chem. 20*, 267−298.
52. Klamt, A., and Schüürmann, G. (1993) COSMO: A New Approach to Dielectric Screening in Solvents with Explicit Expressions for the Screening Energy and Its Gradient, *J. Chem. Soc., Perkin Trans. 2* 799−805.
53. Hartmann, M., Clark, T., and Eldik, R. v. (1997) Hydration and Water Exchange of Zinc(II) Ions. Application of Density Functional Theory, *J. Am. Chem. Soc. 119*, 7843−7850.
54. Suárez, D., Díaz, N., and Merz, K. M., Jr. (2002) Molecular Dynamics Simulations of the Dinuclear Zinc-β-Lactamase from *Bacteroides fragilis* Complexed with Imipenem, *J. Comput. Chem. 23*, 1587−1600.

BI0340191